High sensitivity spectroscopy of the O2 band at 1.27 μm: (I) Pure O2 line parameters above 7920 cm–1

Magdalena Konefal, Samir Kassi, Didier Mondelain, Alain Campargue

High sensitivity spectroscopy of the O_2 band at 1.27 μm: (I) Pure O_2 line parameters above 7920 cm^{-1}.

Magdalena Konefał[1,2], Samir Kassi[1], Didier Mondelain[1], Alain Campargue [1]*

[1] Univ. Grenoble Alpes, CNRS, LIPhy, 38000 Grenoble, France
[2]Institute of Physics, Nicolaus Copernicus University in Toruń, Grudziadzka 5, 87-100 Torun, Poland

Keywords:
Oxygen band at 1.27 μm, Spectral line shapes and intensities; Multispectrumline profile fitting; Cavity ring-down spectroscopy; Absolute frequency measurements; Speed-Dependent Nelkin-Ghatak profile.

*Corresponding author: Alain Campargue (alain.campargue@univ-grenoble-alpes.fr)

Abstract

The atmospheric band of O_2 near 1.27 μm plays an important role in determining the sounded air mass from ground or space borne atmospheric spectra. This band consists of narrow absorption lines of the $a\ ^1\Delta_g - X\ ^3\Sigma_g^-(0-0)$ transitions superimposed to a much broader collision-induced absorption structure. The present contribution is part of a long standing project aiming to improve different aspects of the spectroscopy of this band by highly sensitive cavity ring down spectroscopy (CRDS).

In the present contribution, low pressure (5 and 10 Torr) spectra of pure O_2were recorded with unprecedented sensitivity in the 7920-8085 cm^{-1} interval (noise equivalent absorption, α_{min}, on the order of 10^{-12} cm^{-1}) using an external cavity diode laser. About 170 lines including electric quadrupole transitions were accurately measured. The weakest lines have intensity on the order of 10^{-30} cm/molecule. The coupling of the CRDS spectrometer with a self-referenced frequency comb allows an important gain on the accuracy of the line center determination. Detailed line profile analysis using the quadratic Speed-Dependent Nelkin-Ghatak profile was performed for a series of twelve lines recorded for pressures up to 150 Torr. In particular, the very weak self-pressure shifts (on the order of 10^{-3} cm^{-1}/atm) could be determined for the first time. Line intensities with uncertainty of 1 % are reported for lines with intensity larger than 10^{-28} cm/molecule. Accurate spectroscopic parameters of the $a\ ^1\Delta_g(v=0)$ upper level were fitted to the zero-pressure line centers. An *rms* value of 108 kHz (3.6×10^{-6} cm^{-1}) is achieved for the (meas.-calc.) differences of the $^{16}O_2 a\ ^1\Delta_g(v=0)$ upper level (J_{max}= 37). Significant deviations compared to the HITRAN database are discussed.

1.Introduction

Being a symmetric diatomic molecule, the $^{16}O_2$ oxygen molecule has no dipolar electric moment and thus no electric dipole-allowed vibrational bands. Weak magnetic dipolar transitions are observable in the ground electronic state. They manifest as a fine-structure Q-type branch near 60 GHz as well as a rotational R-type branch in the far infrared and in the region of the (1-0) fundamental vibrational band near 6.5 µm. The oxygen spectrum shows a few electronic bands in the near infrared and visible which are of particular importance for a number of atmospheric applications. The strongest transitions belong to the well-known $b\ ^1\Sigma_g^+ - X\ ^3\Sigma_g^-(0-0)$ A-band near 760 nm which is about 100 times stronger than the $a\ ^1\Delta_g - X\ ^3\Sigma_g^-(0-0)$ band near 1.27 µm considered in this work. Note that electric dipole (E1) transitions are forbidden for these two electronic bands too, as the involved electronic levels have all gerade symmetry. The 760 nm A-band and the 1.27 µm band are thus formed by relatively weak magnetic dipole (M1) transitions and extremely weak electric quadrupole transitions (E2).

As the mixing ratio of oxygen is constant in the Earth's atmosphere, these two bands are valuable to determine the air mass along the line of sight from ground [1] or space borne atmospheric spectra [2, 3]. In particular, the 1.27 µm band is used by the Total Carbon Column Observing Network (TCCON) for ground-based air mass determination [4, 5, 6]. The A-band and the 1.27 µm band were selected by the French space agency, CNES, for the satellite mission MicroCarb [7], dedicated to the accurate determination of column integrated concentrations of CO_2 that should be launched by 2021. The targeted accuracy on the column-averaged CO_2 mole fraction (better than 1 ppm or 0.3 % in relative) requires an accurate derivation of the dry air column from the O_2 column using a constant volume mixing ratio of 0.2095 [8]. Compared to the A-band, the spectral proximity to the used 1.6 µm CO_2 absorption band is an advantage to reduce the uncertainties linked to the correction of surface pressure and aerosol scattering effects [2].Furthermore, the 1.27 µm band has the advantage of having less saturated lines compared to the stronger A-band.

Fig. 1 presents a spectrum of the 1.27 µm band for a pressure of 1 atm of oxygen computed using the HITRAN2016 spectroscopic database [9]. In addition to the M1 and E2 rovibronic absorption lines, the O_2 absorption bands include a broad continuum, namely the collision induced absorption (CIA) continuum due to short-lived collisional O_2-O_2 (and O_2-N_2 in air) complexes. While, lines absorption is proportional to the O_2 density, the self- and foreign components of the CIA are proportional to the squared O_2 density and to the product of O_2 and N_2 densities, respectively. Note that the relative contribution of the CIA and of the lines varies with the considered band [10]. In particular, the CIA of the 1.27 µm band is much stronger than that of the A-band [9, 11].The resulting difference in pressure dependence of the O_2 absorption bands has been proposed as a mean to monitor O_2 in the atmosphere of exoplanets [12].

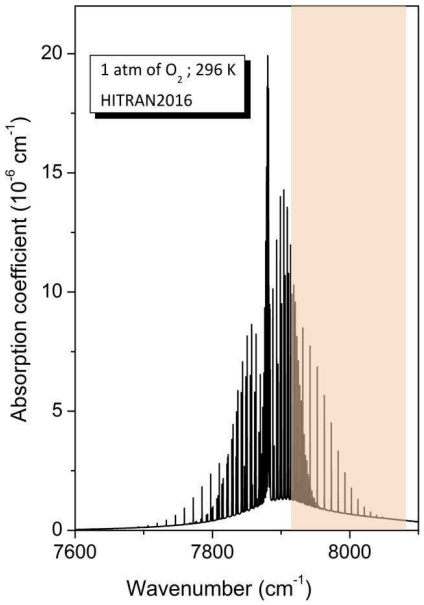

Fig. 1
Simulation of the absorption spectrum of oxygen at 1 atm and 296 K in the region of the 1.27 µm band. (The HITRAN2016 values of the line parameters and of the CIA were used for the simulation). The 7920-8085 cm^{-1} highlighted region is studied in this work while CRDS analysis of the lower range (7658-7917 cm^{-1}) was reported in [13, 14].

The present work is part of a project dedicated to a better characterization of the absorption lines and of the CIA of the 1.27 µm O_2 band in order to fulfill demanding requests for atmospheric applications, in particular for the above mentioned MicroCarb mission. We have recently applied the highly sensitive cavity ring down spectroscopy (CRDS) technique to accurately determine the room temperature CIA binary coefficients from low density spectra (0.36 to 0.85 amagat) of pure oxygen and an O_2/N_2 mixture at room temperature, over the wide 7513-8466 cm^{-1} region [15]. Although more accurate, the obtained binary coefficients were found in agreement with previous measurements by Maté *et al.* using high pressure Fourier transform spectroscopy (FTS) [16]. As concerned absorption lines, the most sensitive previous measurements of pure O_2 spectra were obtained by CRDS a few years ago [13, 17]. In particular, previous identification of E2 quadrupole lines in atmospheric solar spectra acquired with a ground based Fourier transform spectrometer (FTS) was confirmed in the laboratory by CRDS and the obtained quantitative intensity information was used as input data for calculation of a complete list of E2 transitions [17]. A systematic CRDS investigation was performed in the 7658-7917 cm^{-1} region for "natural" and ^{18}O and ^{17}O highly enriched oxygen revealing not only the E2 transitions but also the M1 (1-1) hot band and new high rotational transitions of the (0-0) band of the five most abundant oxygen isotopologues ($^{16}O_2$, $^{16}O^{18}O$, $^{18}O_2$, $^{16}O^{17}O$, $^{17}O^{18}O$ and $^{17}O_2$) [13, 14]. These measurements combined with microwave and Raman data available in the literature allowed improving the determination of the spectroscopic constants

for the $X^3\Sigma_g^-$ and $a^1\Delta_g$ states [13, 14].

Interestingly, the line profiles of low rotational transitions of the ^{17}O-containing isotopologues were observed to be importantly broadened in the room temperature spectra (recorded with a few tens Torr pressure) [13]. This effect is related to the non-zero nuclear spin of the ^{17}O nucleus (I= 5/2) resulting in significant nuclear-spin orbit hyperfine (hf) splitting of the upper energy levels. CRDS recordings with a cryogenic cell at 80 K allows for a significantly better resolution of the hf structure [18]. The rotational and hf spectroscopic parameters derived from these measurements and literature data, allowed for a very good reproduction of the spectra including the hf multiplets [14].

These previous CRDS studies of pure O_2 spectra were thus mostly dedicated to weak lines and new observations with marginal impact for atmospheric simulations. More important are the line parameters (position, intensity and broadening coefficients) of the relatively strong M1 transitions which remain insufficiently characterized. For instance, line intensities retrieved from previous FTS works with long path absorption cell [19] are provided with a typical 10 % error bar in the current edition of the HITRAN database [9]. Indeed, due to the weak absorption of the considered band (line intensities are less than 1×10^{-25} cm/molecule), the derivation of precise line parameters from FTS spectra is very challenging. Previous FTS line shape studies [19-21] were all limited to the standard Voigt profile analysis. As concerned pressure line shifts, only an upper limit of the pressure line shift could be estimated from FTS spectra up to 3 bar [22]. Conversely, the line profiles of the (stronger) A-band transitions have been recently the subject of important efforts in support of the OCO-2 mission, using both FTS and CRDS (see [23] and references quoted therein). Note that in its present version, the HITRAN2016 database provides for the 1.27 μm band, line profile parameters transferred from …the A-band [4, 24].

In the present contribution, we use an improved CRDS setup to investigate at very high sensitivity the high energy region above 7920 cm^{-1}, which was not studied in our previous CRDS studies (see **Fig. 1**). While a series of fibered distributed feedback (DFB) lasers were previously used as light source below 7920 cm^{-1} [13, 14], an external cavity diode laser (ECDL) is adopted in the present work for a more efficient light injection into the CRDS cell. In addition, following previous works, ([25, 26]), the CRD spectrometer is coupled to a self-referenced frequency comb (SRFC) providing accurate frequency value for each ring down event. As a result, a gain in sensitivity of more than one order of magnitude (noise equivalent absorption $\alpha_{min}\sim 10^{-12}$ cm^{-1}) is achieved leading to better quality line profile determination and allowing for low pressure recordings at a few Torr, valuable for an accurate determination of the zero-pressure line centers and of the line intensities.

Series of spectra of pure O_2 were recorded in view of the determination of the center, intensities, self-pressure shifts and self-broadening parameters. A continuous spectrum recording with natural oxygen over the 7920-8085 cm^{-1} interval was performed for pressure values of 5.0 and 10.0 Torr, leading to the

observation of more than 160 lines of the $^{16}O_2$, $^{16}O^{18}O$ and $^{16}O^{17}O$ isotopologues in normal isotopic abundance. In spite of the low pressure of the recordings, the measured line profiles exhibit clear deviations from the standard Voigt profile. In order to determine the best suited line profile, a detailed line profile analysis was undertaken for twelve selected lines recorded for a series of pressures up to 150 Torr. Using a multispectra treatment (see [27, 28]) a satisfactory reproduction of the series of recordings was achieved with the quadratic speed-dependent Nelkin-Ghatak profile (qSDNGP). As a result, an empirical dependence of the qSDNGP parameters *versus* the upper rotational quantum number was determined from the twelve lines. Then, the resulting qSDNGP profile with constrained profile parameters was used to determine the line centers and line intensities of all the lines of the 5 and 10 Torr spectra. In the Discussion section, the obtained results, in particular position and intensities, are compared to literature values. Accurate spectroscopic constants of the $a\ ^1\Delta_g(v=0)$ upper level of $^{16}O_2$ and $^{16}O^{18}O$ are determined from a fit of the zero-pressure line centers, providing accurate line positions not only in the considered spectral region but for the whole absorption band.

The experimental setup and the performances achieved are described in the next Section. The line profile analyses using the speed-dependent Nelkin-Ghatak profile is presented in Section 3. The obtained results are discussed and compared with literature in Section 4 before the concluding remarks (Section 5).

2. CRDS recordings

2.1. Spectra acquisition

Except the use of an external cavity diode laser (ECDL) rather than a distributed feedback (DFB) laser diode, the optical setup is mostly similar to those described in Refs. [29-32]. A sketch of the experimental arrangement is presented in **Fig. 2**. The “on the fly” measurement of the laser frequency values associated to each ring down event by coupling with a self-referenced OFC was first implemented in Refs. [33-35].

The CRD system, except the laser source, was installed in a protective Plexiglas enclosure. The stainless steel gas cell was covered with a tube of insulation foam. Its temperature was monitored with a PT 1000 resistive probe (class Y, ±0.15 K accuracy at room temperature) and an analog temperature sensor (TSic 501, IST-AG, ±0.1 K accuracy) both fixed on the cell surface. In order to limit the amount of desorbed water vapor in the CRDS cell, the spectra were recorded in flow regime. The flow (not monitored) was adjusted to roughly 5 sccm with a downstream manual needle valve. Controlling an upstream solenoid valve, the pressure was actively PI regulated using either a 10 Torr or 1000 Torr capacitance gauge (MKS Baratron, 0.15% accuracy of the reading) according the total pressure.The regulation noise was 20 ppm at 10 Torr.

The ECDL light is first sent into a polarization maintained fiber coupler (PFC, 90/10), which directs about 10% of the emitted light to a frequency measurement setup and the remaining 90% into a fibered

acousto-optic modulator (AOM) driven at RF frequency f_{AOM}, inserted before the 1.4-meter-long high-finesse cavity (HFC) ($F \approx$ 130,000).The AOM, used on its order +1, interrupts the excitation once resonance with one of its longitudinal modes is achieved, leading to a ring down (RD) event. Each RD is detected with an InGaAs photodiode. Similarly to our previous realization [36], the resonance is sought by adjusting the length of the cavity over λ/2 with a piezo-electric tube (PZT_C) that hosts the output mirror. A fast modulation (50 Hz) spanning 5% of the cavity free spectral range (FSR) is superimposed to the PZT_C control voltage, which is slowly (1s full span) ramped over an FSR until a first RD event occurs. It is then locked to this position using a Proportional Integral (PI) locking software procedure that acts on the offset voltage, until enough RD events are recorded.

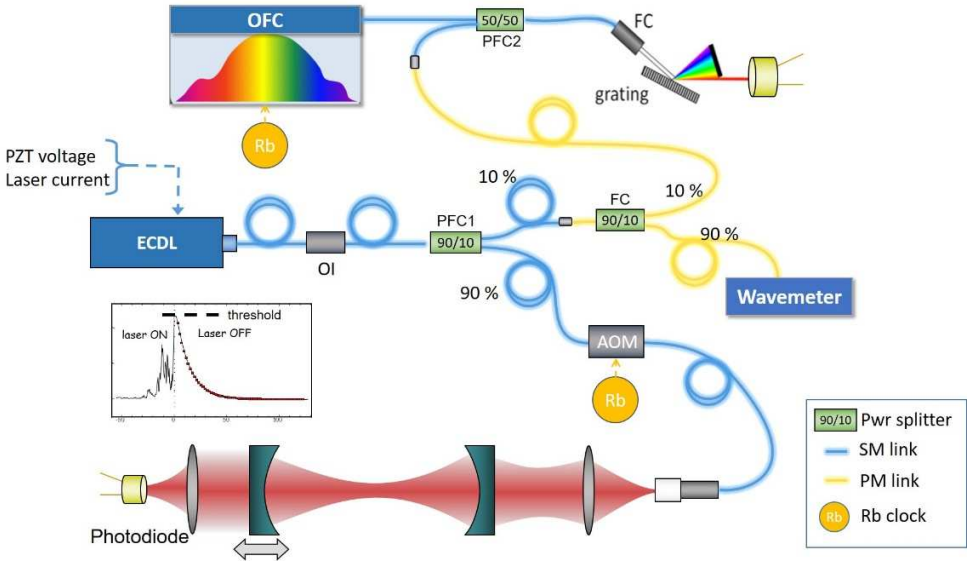

Fig. 2

Scheme of the CRD spectrometer coupled with the self-referenced optical frequency comb (OFC). The different components include an external cavity diode laser (ECDL), an optical isolator (OI), a fiber coupler (FC), two polarization maintained fiber couplers (PFC1,2), the OFC and acousto-optic modulator (AOM) referenced to a GPS referenced rubidium (Rb) clock.

The absolute ECDL emission frequency f_{ECDL} is determined from:

$$f_{ECDL} = f_{CEO} + n f_{rep} \pm f_{BN} \quad (1)$$

Where the repetition rate f_{rep} and the carrier-envelope offset frequency f_{CEO} are locked to 250 MHz and 20 MHz, respectively, with a relative uncertainty of 10^{-11}. The number n of the tooth with which the ECDL is beating is deduced from the ECDL emission frequency measured by a Fizeau wavemeter (High Finesse WS-U-30 IR). The 5 MHz resolution and 20 MHz accuracy of this instrument are sufficient to determine unambiguously n as two consecutive teeth are separated by 250 MHz. The beat-note (BN) signal was recorded with a fast ADC (250 MHz sampling rate), and the peak frequency f_{BN} was obtained

after Fourier transform (with a 7 kHz resolution) of the acquired signal. This beat note frequency, f_{BN}, provided with a refresh rate of one thousand times per second, was used to act on the ECDL frequency with a PI software procedure, to stabilize its emission frequency to a given BN frequency set-point. This mechanism ensured laser emission frequency stabilization to 300 kHz rms corresponding to the uncertainty on the absolute laser emission frequency. The beat-note sign is deduced according to the proximity of the absolute frequency to the wavemeter raw value. Note that the OFC-RF electronics, ADC clock and AOM frequency synthesizer were referenced to a GPS referenced 10 MHz rubidium clock.

Because of the AOM, the high-finesse cavity excitation optical frequency is:

$$f_{Exp} = f_{ECDL} + f_{AOM} \tag{2}$$

The ECDL (from Toptica) was tuned by acting on its internal grating angular position and the laser chip current, in an electronically-controlled laser-current-feed-forward scheme. The grating angular position can be roughly set with an external step motor and finely adjusted with an internal piezo electric element (PZT_L). The ECDL has a mode-hop-free tuning range limited to 0.8 cm^{-1} obtained with a linear scan of the PZT_L voltage over about 80% of its full range capability. Broadband spectra were therefore obtained by concatenation of series of slightly overlapping individual narrow spectra. During automatic broadband acquisition, the laser frequency was iteratively stepped by about 0.5 cm^{-1}, by acting on the grating with the step motor. A mode-hop-free scanning situation was then automatically sought by adjusting the PZT_L ramp offset over successive fast (1s) test scans. The instantaneous laser frequency and the Fizeau wavemeter raw signals were used as mode hop free and monomode emission criterion, respectively. Once the optimal PZT_L voltage offset was determined, a 10 minutes long, ~60 MHz step by step scan was started. After each frequency jump, the laser was actively locked using the refreshed BN frequency as a reference, until 40 RDs (~80 Hz repetition rate) were acquired. The lock was then released in order to allow for to a new step. Instead of forcing the BN set-points to pre-defined frequencies, we preferred to set it to its effective value, 100 ms after the jump.

Two different RD averaging scheme were used. For broadband scans, the single laser frequency RD dataset were averaged “on the fly”, together with the BN frequency in order to generate small size individual spectra. Occasionally, when the BN frequency was too close from the 0 or 125 MHz limit, its sign could not be determined. These spectral points were then rejected. In the case of individual high resolution recordings dedicated to line profile analysis, every single RD event was recorded together with experimental parameters, including BN, instantaneous raw wavelength, cell pressure, cell temperature and ECDL scan parameters, leading to heavy data files. The benefit was that the post-processing of RD event and BN packets was lossless. In addition, we could verify that the BN - thus the laser frequency - was steady during each acquisition step and that RD events statistics was regular.

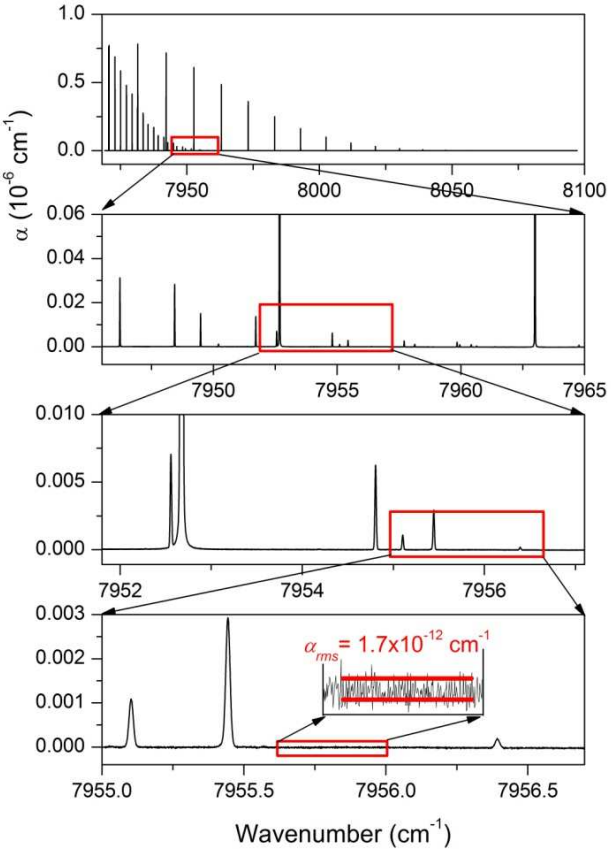

Fig. 3
CRDS spectrum of O_2 between 7919.8 and 8085.3 cm^{-1} at 10 Torr. The successive enlargements illustrate the sensitivity and high dynamical range of the recordings: absorption coefficients are determined from a value close to 10^{-6} cm^{-1} down to the noise level of about 1.7×10^{-12} cm^{-1}.

As mentioned above, the following analysis is based on two series of recordings with pure oxygen (AlphaGaz2 from Air Liquide, purity≥ 99.9995 %):

(i) Two wide spectra covering continuously the entire 7920-8085 cm^{-1} region with pressure values of 5.0 and 10.0 Torr. During the 5 Torr spectrum measurements, the cell temperature fluctuated between 294.33 and 295.89 K and during the 10 Torr spectrum measurements between 294.34 and 295.38 K. The pressure stability was at the level 6×10^{-4} Torr for both recordings.

(ii) Series of spectra at different pressures were recorded over a 0.78 cm^{-1} interval around 12 lines selected for a detailed line profile analysis. In general, the pressure range was 5-150 Torr with, in principle, four additional intermediate pressure values (10, 50, 75, 100 Torr). The temperature stability is at the level of from 0.025 to 0.07 K, except for the S7R8line for which variations up 0.11 K (due to an air conditioning problem) are noted. The pressure stability is from about 10^{-4} Torr for the lowest measured pressures to 2×10^{-2}Torr for spectra at 150 Torr.

In all the recordings, the sampling step was chosen to be about 6×10^{-4} cm^{-1} to be compared to a Doppler line width of about 8.5×10^{-3} cm^{-1} (HWHM). The number of RD events averaged for each spectral point was 40 or 100 for broadband spectra. In the case of the line profile study, the number of RD (with a minimum value of 40) was increased on the line profile in order to achieve a similar noise level on the line and on the nearby baseline. **Fig. 3** illustrates the sensitivity and high dynamical range on the intensity scale of the 10.0 Torr spectrum. The noise equivalent absorption evaluated as the *rms* of the baseline fluctuations is around 2×10^{-12} cm^{-1}.

2.2. Overview of the observations

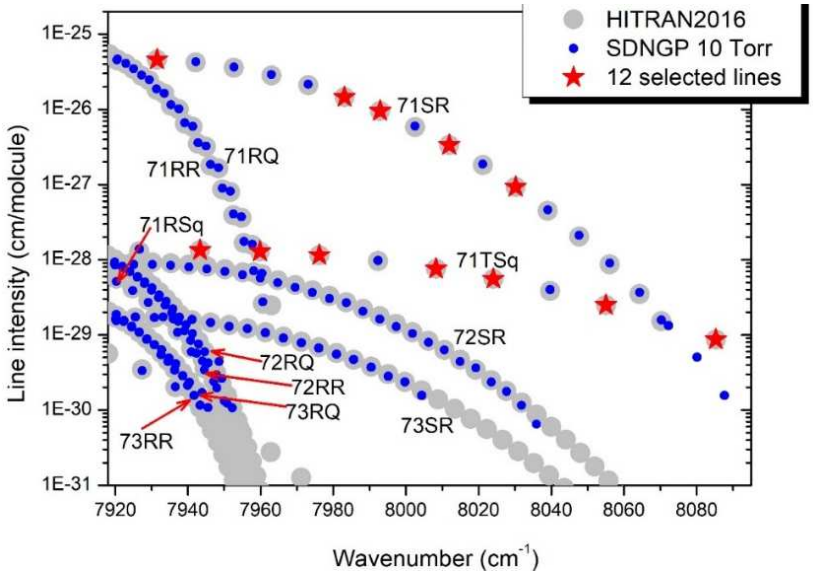

Fig. 4
Overview of the $a^1\Delta_g - X^3\Sigma_g^-$ line listas provided by HITRAN2016 (full grey dots) [9] in the 7920-8075 cm^{-1} region for oxygen in natural abundance. The lines measured by CRDS at 10 Torr (SDNGP fit, blue dots) and the 12 lines selected for multi-pressure recordings (red stars) are indicated. Following HITRAN notation, the $^{16}O_2$, $^{16}O^{18}O$ and $^{16}O^{17}O$ lines are labeled 71, 72 and 73, respectively (The 71RS and 71TS branches correspond to quadrupolar electric transitions (q)).

Let us recall that each rotational level (*N*) of the ground $X^3\Sigma_g^-$ state of O_2 splits into three spin-components as the O_2 molecule has two unpaired electrons with parallel spin which sum up to the total electron spin *S*=1. It leads to a triplet multiplicity with total angular momentum *J*= *N*-1, *N* or *N*+1. In the $a^1\Delta_g$ electronic excited state, the total electron spin is equal to 0 and the *N* value corresponds to *J*. Note that for the $^{16}O_2$ main isotopologue, only odd rotational levels exist in the ground state. The magnetic dipole (M1) transitions follow the ΔJ= 0, ±1 selection rule leading to the observation of nine $\Delta N(N)\Delta J(J)$ branches: [*OP*,*PP*,*QP*], [*PQ*, *QQ*,*RQ*] and [*QR*, *RR*, *SR*]corresponding to ΔJ= -1, 0 and +1, respectively (see Fig. 4 of [17]). Electric quadrupole (E2) transitions follow the ΔJ= 0, ±1, ±2 selection rule, which leads to 15 possible branches, but the ΔJ = 0, ±1 E2 lines coincide with the much stronger M1 lines and

cannot be separated. Therefore, only the [*NO*,*OO*,*PO*] and [*RS*, *SS*, *TS*] branches with ΔJ= -2 and +2, respectively, are measurable. In fact, no E2 transitions belonging to the *OO* and *SS* branches were detected so far.

Table 1
Overview of the assignments of the CRDS observations of the $a^1\Delta_g - X^3\Sigma_g^-$ transitions of O_2 in the 7919.8 -8085.3 cm^{-1} range. For each branch, the range of *J* values corresponding to the measured transitions is given.

Branch[a]	$^{16}O_2$	$^{16}O^{18}O$	$^{16}O^{17}O$
S*(N=J-1)*R*(N=J) d*	6 ≤ *J*≤ 42	6≤ *J*≤ 31	6≤ *J*≤ 23
R*(N=J)*R *(N=J) d*	15≤ *J*≤ 37	14≤ *J*≤ 31	14≤ *J*≤ 26
R*(N=J-1)*Q*(N=J) d*	14≤ *J*≤ 36	14≤ *J*≤ 32	14≤ *J*≤ 26
T*(N=J-1)*S*(N=J) q*	4≤ *J*≤ 24		
R*(N=J)*S*(N=J-1) q*	13≤ *J*≤ 27		
Nb of lines	65[b]	62	40

Notes:
[a] The notations *d* and *q* correspond to magnetic dipole (M1) and electric quadrupole (E2) transitions, respectively. Strictly speaking, *d* branches include a small contribution due to E2 transitions (see Text).
[b] Including three lines of the (1-1) hot band and three lines not included in HITRAN2016 (S37R38, S39R40 and S41R42).

The assignment of the O_2 lines by comparison to the HITRAN2016 (calculated) line list was straightforward (see **Fig. 3**). Overall, 65, 62 and 40 transitions of the $^{16}O_2$, $^{16}O^{18}O$ and $^{16}O^{17}O$ isotopologues in natural isotopic abundance (0.99526, 3.99×10^{-3}, 7.4×10^{-4} respectively) were identified (see **Table 1**). The $^{16}O_2$ transitions include nineteen E2 transitions of the *RS* and *TS* branches and three transitions of the (1-1) hot band. Note that in spite of the relatively low pressure values of the recordings, lines with intensity on the order of 1×10^{-30} cm/molecule could be measured. The HITRAN list includes lines with intensity down to 10^{-31} cm/molecule. Nevertheless, the S37R38, S39R40and S41R42lines around 8080 cm^{-1} with intensity larger than 10^{-30} cm/molecule were detected while they are absent in the HITRAN list, probably due to a high *J* value cut-off.

3. Line profile analysis

3.1. Voigt profile

In a first step, we considered separately the 5 and 10 Torr spectra and constructed the corresponding line lists assuming the usual Voigt profile (VP) for the line shape as this profile remains the most commonly used. The spectra were fitted using a homemade multi-line fitting program written in LabVIEW and C++. The Doppler width was fixed to the theoretical value calculated according to the temperature value and the isotopologue mass. The line intensity was then converted to the 296 K reference

temperature according to the lower state energy value and partition functions provided by the HITRAN2016 list [9].

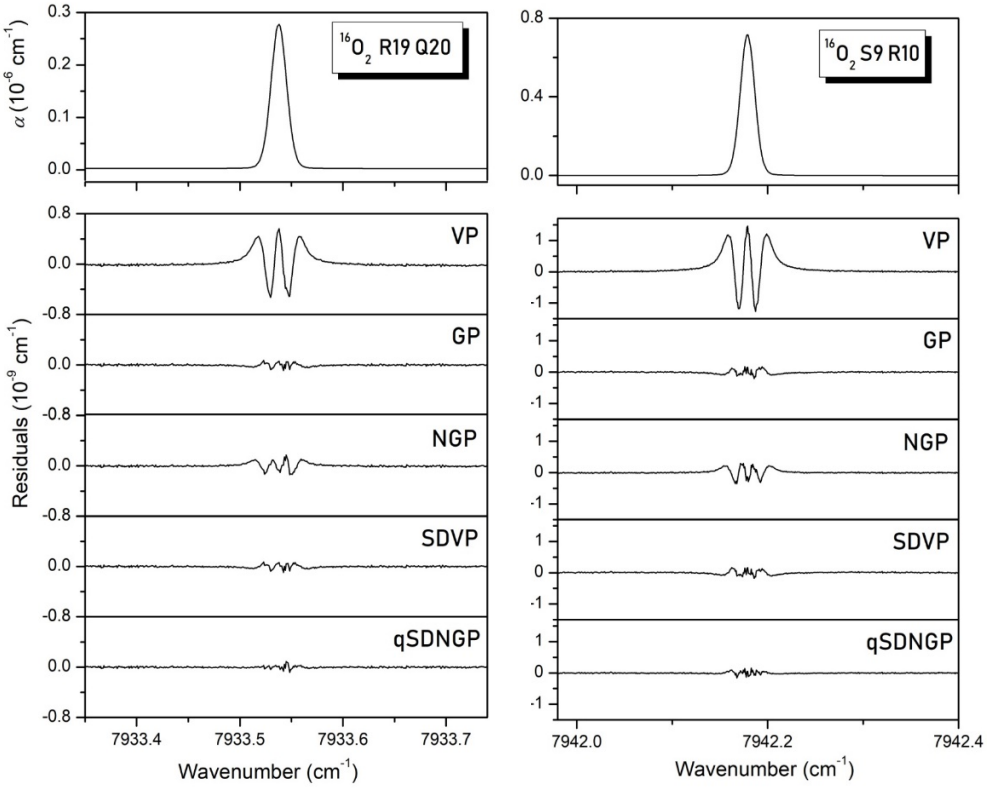

Fig. 5
Example of fit residuals of two $^{16}O_2$ lines at 10 Torr for different line profiles.

A VP list of 167 and 164 lines was retrieved from the spectra at 10 and 5 Torr, respectively. The two lists including line position, line intensity and collisional width values are provided as Supplementary Material. Let us underline that the two fits were performed independently and the obtained line positions are thus including the pressure shift at measurement pressure. As illustrated in **Fig. 5**, the VP is not sufficient to reproduce the line profiles at 5 and 10 Torr and a more sophisticated line shape is required. The VP residuals exhibit a W shape which is the usual signature of collisional narrowing effects. Indeed, most of the residuals vanish by using a Galatry profile (GP) [37] or a Nelkin-Ghatak profile (NGP) [38, 39] which accounts for the collisional narrowing assuming a soft-and hard-collision model, respectively. The residuals obtained with a Speed-Dependent Voigt Profile (SDVP) [40] and a quadratic Speed-Dependent NGP (qSDNGP) [41, 42] are also displayed in **Fig. 5**. Interestingly, the GP and SDVP fit residuals are similar in spite of different fitted parameters. NGP gives twice larger residuals than GP while the set of fitted parameters is identical. Although showing significant deviations up to one or two orders of

magnitude above the noise level, the qSDNGP allows the best line shape reproduction. Both the speed dependence of pressure broadening and shifting and the collisional narrowing (in the hard collision model) parameters are adjusted in the qSDNGP. It is worth noting that while the VP residuals are large, they do not show clear asymmetry and thus the fitted values of the VP and qSDNGP line centers are expected to be close (see Section 4). Note that the qSDNGP with a correlation parameter, known as the Hartmann-Tran profile (HTP), is the profile recommended for future implementation in spectroscopic databases [43].

In summary, the qSDNGP is found to be the most suitable profile to reproduce the recorded spectra. Nevertheless, considering the small pressure difference, the two available recordings at 5.0 and 10.0 Torr are sometimes insufficient to retrieve physically meaningful values of the seven qSDNGP parameters required to be fitted for each line. This is why we undertook a detailed line profile study of a selected set of lines over a larger pressure range in order to determine more reliable values of the line parameters (*e.g.* pressure shift). From this selected set of qSDNGP parameters, empirical dependence *versus* the rotational quantum number will be determined and used as constraints for a qSDNGP fit of all the lines observed in the spectra at 5.0 and 10.0 Torr.

3.2 Multi-pressure analysis of the selected lines

Five M1 lines of the SR branch and seven E2 lines of the TS branch of $^{16}O_2$ with J values ranging from 5 to 27 were chosen for recordings with pressures up to 150 Torr. They are listed in **Table 2** and highlighted on **Fig. 4**. The absence of overlapping with nearby lines (in particular due to water vapor present as an impurity), the range of J values and the intensity were used as criteria for the selection. In addition to the Doppler width (Γ_D), pressure broadening (Γ_0) and pressure-shift (Δ_0) parameters which are common to all the profiles, the qSDNG parameters include the quadratic speed dependence of the pressure width and shift (Γ_2 and Δ_2) and the Dicke narrowing parameter(ν_{vc}) [44].A multispectrum fitting procedure in which parameters for lines recorded at different pressures are simultaneously adjusted, was used to retrieve the (ν_0, S_{296K}, Γ_0, Δ_0,Γ_2, Δ_2,ν_{vc}) parameters of the considered lines. The multispectrum fitting of high S/N spectra recorded in an appropriately large dynamic pressure range helps reducing the correlation between the fitted parameters *e.g.* between Γ_2 and ν_{vc}. The used fitting code is a homemade program written in LabVIEW and C++. The fitting procedure, based on the Minuit2 routine from CERN, minimizes the residuals *rms* of all fitted multi-pressure spectra.

An example of residuals obtained using a multispectrum fit with the Voigt, NG and qSDNG profiles is shown in **Fig. 6** for the S19R20line recorded at seven pressures between 5 and 150 Torr. The clear asymmetry of the NGP residuals, increasing with pressure, is a manifestation of speed-dependent effects which are well accounted for by the qSDNGP.

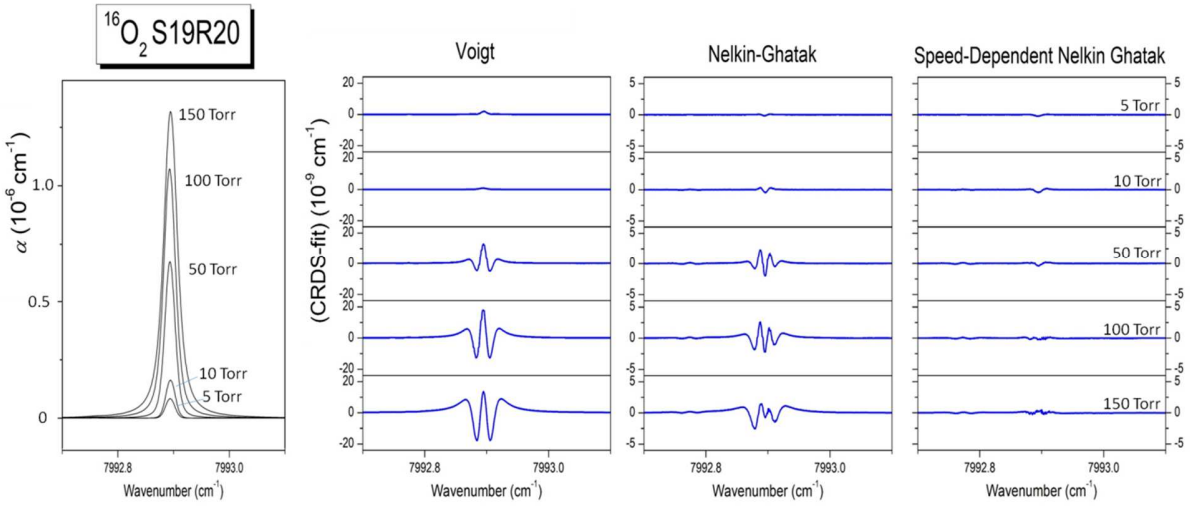

Fig. 6

Spectra of theS19R20 line of $^{16}O_2$ for a series of pressure between 5 and 150 Torr and corresponding residuals obtained by a multispectrum fit using Voigt, Nelkin-Ghatak and quadratic speed-dependent Nelkin-Ghatak profiles. Note that the absorption spectrum is plotted in 10^{-6} cm^{-1} unit while residuals are plotted in 10^{-9} cm^{-1} unit and that a different ordinate scale is used for the Voigt profile. The asymmetry of the NGP residuals shows the importance of speed-dependent effects.

The fitted values of the multispectrum qSDNGP parameters of the selected lines are given in **Table 2**.

The used multispectrum fitting program did not provide statistical error bar on the fitted values of the different parameters. In order to estimate the fitting error on the zero-pressure positions, we performed independent fit of each spectrum with free position and the (S_{296K}, Γ_0, Γ_2, Δ_2, ν_{vc}) set of parameters fixed to the values of **Table 2**. As an illustration of the consistency of the treatment, **Fig. 7** (left panel) shows the pressure dependence of the retrieved pressure shifts for the five selected SR lines. The error bars on the zero-pressure position included in **Table 2** correspond to the statistical error obtained from a linear regression *versus* pressure. Their values range between 16 kHz and 1.2 MHz (less than 50 kHz for the five SR lines).

A similar procedure was followed for the line intensities: all parameters, except S_{296K}, being fixed to their value of **Table 2**, the intensity value was fitted for each spectrum. The intensity error bars given in **Table 2** correspond to the standard deviation of retrieved intensities. The agreement of the intensity values retrieved at different pressures is at the 1‰ level **(Fig. 7**, right panel), except for the 5‰ excess of a few measurements of the S7R8 line (related to an air conditioning problem).

Table 2

Parameters derived for the twelve $^{16}O_2$ lines in the SR (dipolar) and TS (quadrupolar) branches analyzed using a multi-pressure fit.

Line	ν_0 (cm^{-1})	S_{296K} (cm/molecule)	Γ_0 (cm^{-1} $Torr^{-1}$)	Δ_0 (cm^{-1} $Torr^{-1}$)	Γ_2 (cm^{-1} $Torr^{-1}$)	Δ_2 (cm^{-1} $Torr^{-1}$)	ν_{vc} (cm^{-1} $Torr^{-1}$)	*P* range (Torr)
S7R8	7931.51032391(54)	4.672(17)E-26	6.46E-5	2.55E-7	5.40E-6	6.49E-8	3.10E-6	5-40
S17R18	7983.1113247(18)	1.4991(17)E-26	5.69E-5	-6.34E-7	4.92E-6	2.15E-7	3.37E-6	5-150
S19R20	7992.8979892(12)	9.7701(77)E-27	5.47E-5	-8.09E-7	3.18E-6	2.22E-7	7.40E-6	5-150
S23R24	8011.9166511(14)	3.4530(43)E-27	5.12E-5	-1.11E-6	5.14E-6	2.25E-7	3.70E-6	5-150
S27R28	8030.1754833(17)	9.582(12)E-28	4.72E-5	-1.43E-6	5.36E-6	2.57E-7	3.91E-6	5-160
T5S6	7943.3447493(35)	1.3339(35)E-28	6.43E-5	8.96E-7	1.00E-7	2.59E-7	9.45E-6	5-50
T7S8	7959.8467071(35)	1.2755(56)E-28	6.34E-5	9.14E-7	5.41E-7	3.47E-7	1.11E-5	5-150
T9S10	7976.1717370(47)	1.1628(14)E-28	6.17E-5	6.91E-7	3.14E-7	4.52E-7	1.15E-5	5-150
T13S14	8008.2845747(59)	7.669(21)E-29	5.85E-5	-3.63E-8	4.13E-7	5.49E-8	1.21E-5	5-150
T15S16	8024.066710(24)	5.688(12)E-29	5.66E-5	-5.31E-8	3.80E-7	1.88E-7	1.15E-5	5-150
T19S20	8055.065516(24)	2.5522(37)E-29	5.25E-5	-1.05E-7	4.27E-7	2.61E-7	1.15E-5	5-150
T23 S24	8085.282656(42)	8.910(57)E-30	4.69E-5	-4.13E-7	1.80E-7	3.43E-7	9.18E-6	5-150

Note

The uncertainty on the zero-pressure line positions (ν_0) and on the line intensities (S_{296K}) are given in the unit of the last quoted digit and corresponds to statistical errors (1σ) (see Text).

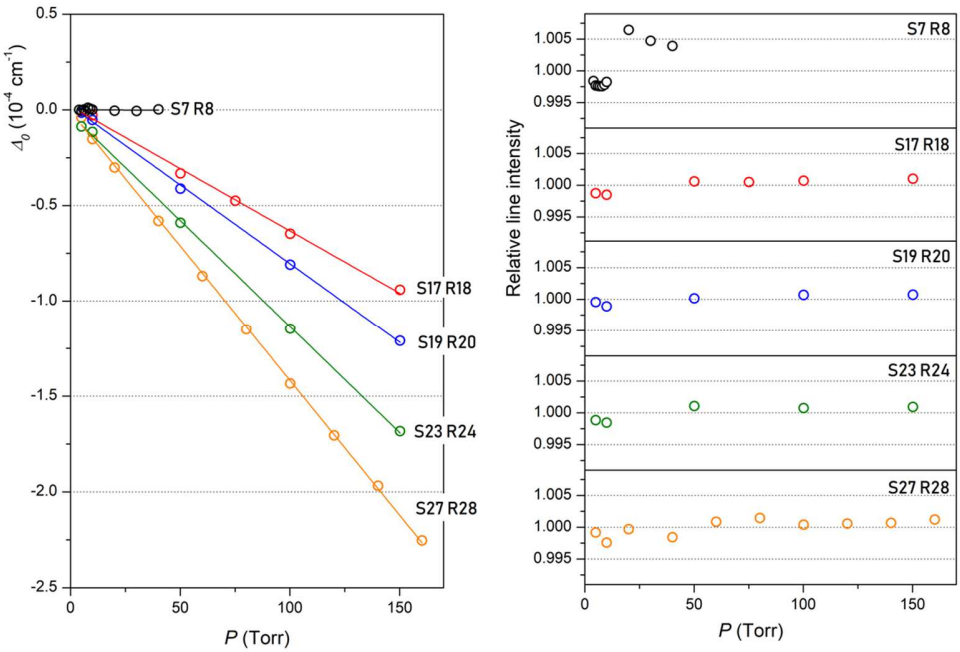

Fig. 7
Pressure dependence of the position shifts (Δ_0) and of the line intensities (S_{296K}) obtained by the qSDNGP multispectrum fit for the five SR lines selected.

The J' dependence of the Γ_0, Δ_0 and Δ_2 line-shape parameters of the twelve selected lines is presented in **Fig. 8**. The pressure-shift and pressure-broadening parameters show a mostly linear J' dependence for J' between 8 and 37. The Γ_2 parameter is known to be strongly correlated with the Dicke narrowing parameter (ν_{vc}) [45, 46] which leads to a large dispersion of values in particular for the weaker TS E2 lines. This correlation is illustrated by the ν_{vc} values obtained for S17R18 and S19R20 which differ by a factor of 2 and seem anticorrelated with Γ_2 values (see **Table 2**). Thus the physical significance of ν_{vc} and Γ_2 parameters as obtained in our treatment is probably limited.

The strongest SR lines were mainly used to fix the empirical J' dependence of the line-shape parameters required for the treatment of all the lines observed in the spectra at 5 and 10 Torr. As a result, the following empirical expressions were obtained (all values in $cm^{-1}Torr^{-1}$): $\Gamma_0 = 7.28\times10^{-5}-8.67\times10^{-7}J'$, $\Delta_0 = 9.93\times10^{-7}-8.44\times10^{-8}J'$, $\Delta_2 = 2.21\times10^{-7}$, $\Gamma_2 = 5.30\times10^{-6}$, $\nu_{vc} = 3.53\times10^{-6}$. The empirical J dependence of Γ_0, Δ_0 and Δ_2 are plotted in **Fig. 8** (red solid lines).

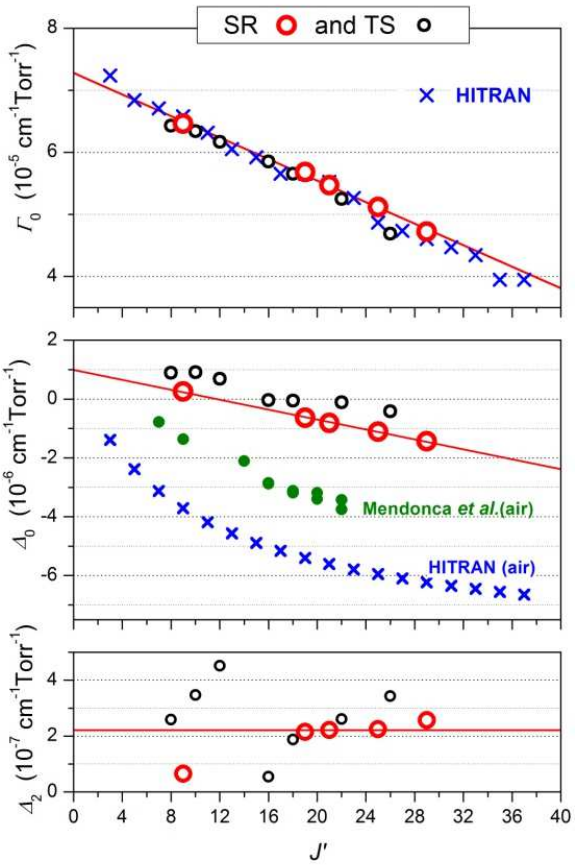

Fig. 8

Dependence of the multi-pressure qSDNGP fitted values of Γ_0, Δ_0 and Δ_2 of the five SR and seven TS lines *versus* the upper total angular momentum, *J'* (red and black open circles, respectively). Values provided in HITRAN2016 and by Mendonca *et al.* [6] are included for comparison (red crosses and green full circles, respectively). Note that the displayed Δ_0 pressure shifts are the air-pressure shifts for HITRAN2016 and Mendonca *et al*. The red lines correspond to the empirical laws used as constraints in the treatment of the global spectra at 5 and 10 Torr.

Constraining the line shape profile according to these empirical laws, the qSDNGP zero-pressure positions and line intensities were determined from independent fit of the lines observed at5 and 10 Torr. The $^{16}O_2$ empirical laws were also adopted for the $^{16}O^{18}O$ and $^{16}O^{17}O$ isotopologues. As all the observed $^{16}O^{17}O$ transitions have *J'*> 7, their hyperfine structure has a marginal impact on the room temperature line profile [14]. The obtained qSDNGP lists at 5 and 10 Torr are included in the same Supplementary Material as the VP line lists.

A conservative 500 kHz accuracy is estimated for the zero-pressure line positions of isolated lines with intensity larger than 10^{-28} cm/molecule. Only a rough estimation can be provided for the accuracy of our intensity values of our two global qSDNGP lists. In addition to the pressure (0.25%) and temperature uncertainties (0.15 K), biases due to the choice of the line profile must be considered. Our results were

obtained from spectra recorded with a maximum pressure of 150 Torr. The use of relatively small pressure values helps to minimize biases related to the profile. As a test of our intensity values, we considered the S27R28 line of the main isotopologue with intensity of 9.28×10^{-28} cm/molecule which was recorded at 500 Torr. Its line intensity at 500 Torr was obtained using the above empirical laws on the line parameters derived in the 0-150 Torr range. Small but significant residuals were obtained from the fit revealing some deviations from the empirical laws. Nevertheless, the line intensity was found to deviate by no more than 0.24 % from its low pressure value. Note that the consistency of the intensity values derived from spectra at different pressures is at the 0.1 % level for four of the five lines displayed in **Fig. 7**. Overall, a 1 % uncertainty seems to be a reasonable estimate of the total error on the reported intensities for the lines with intensities larger than 10^{-28} cm/molecule.

4. Discussion. Comparison with literature.

4.1. Line positions

We recall that contrary to the qSDNGP positions which are empirically corrected from the pressure shifts, the VP positions of our global lists were obtained from independent fits (Section 3.1) and thus include the pressure shifts at 5 or 10 Torr. The (qSDNGP-VP) position differences at 10 Torr plotted *versus J'* in **Fig. 9** illustrate thus the pressure shifts at 10 Torr. The observed linear increase of the deviations for *J'* values up to 40 coincides and thus validates the empirical linear law determined above from five SR lines (red line in **Fig. 9**).

Fig. 9 includes a comparison to the HITRAN2016 line positions. The HITRAN line positions of the $a\ ^1\Delta_g - X\ ^3\Sigma_g^-(0-0)$ band of $^{16}O_2$ were calculated by difference of the energy levels of $a\ ^1\Delta_g(0)$ and $X\ ^3\Sigma_g^-(0)$ states obtained by Yu *et al.* [47] from an isotopically invariant Dunham fit of all the O_2transitions available in the literature. Only three experimental sources of $a\ ^1\Delta_g - X\ ^3\Sigma_g^-(0-0)$line positions were available and used by Yu *et al.*: FTS values measured in emission by Amiot and Vergès [48], FTS absorption values obtained with long path absorption and pressure up to 1.06 bar by Cheah *et al.* [21] and our CRDS results obtained at a pressure of 50 Torr [13]. Overall, a reasonable agreement is obtained between the HITRAN2016 positions and the present accurate measurements, HITRAN deviations decreasing from about to 2×10^{-4} cm^{-1} (6 MHz) for low *J'* values to a practically zero value around *J'*= 36. Nevertheless, for most of the lines, the deviations exceed the 10^{-4} cm^{-1} error bar attached to HITRAN positions. Let us mention that the calculated transition frequencies reported in [13] are larger than HITRAN values by 2.5×10^{-4} cm^{-1} leading to a consistency at the 5×10^{-5} cm^{-1} level with present measurements.

In their paper, Mendonca *et al.* [6] indicated that their line positions originate from [13] but our comparison shows that they are larger by a mostly constant value of 4.3×10^{-4} cm^{-1} compared to the

475 calculated values included in [13] (+6.8×10^{-4} cm^{-1} compared to HITRAN). It leads to differences between
476 5×10^{-4} cm^{-1} and 7×10^{-4} cm^{-1}, compared to the present values (see **Fig. 9**).
477

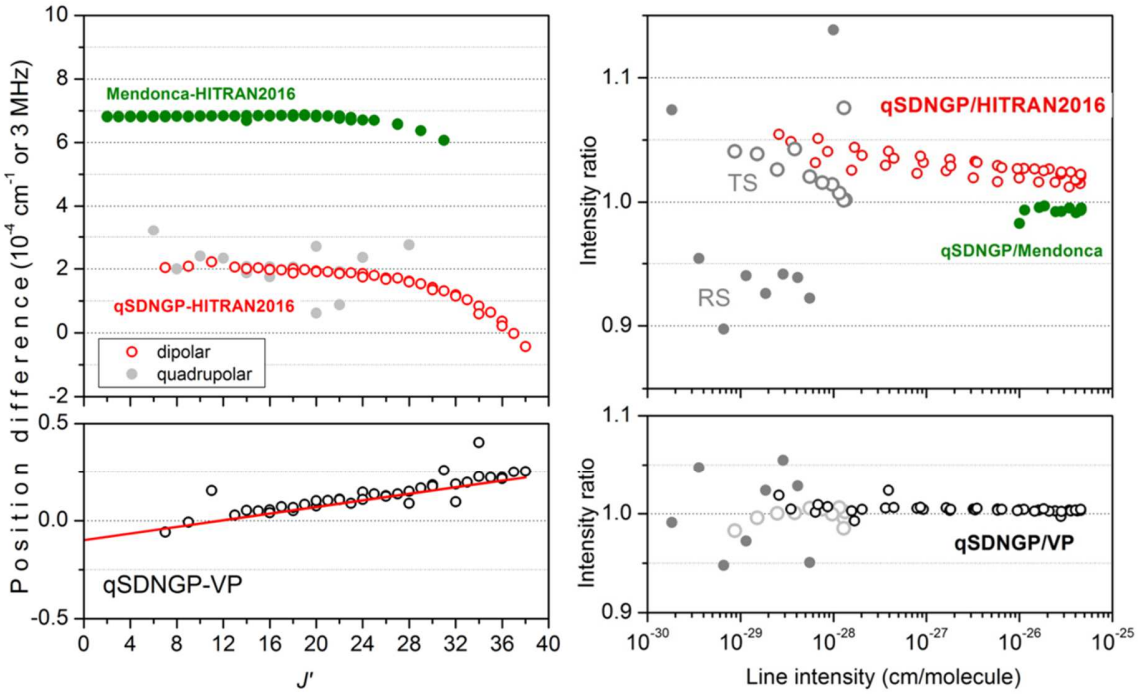

478
479 **Fig. 9**
480 Position differences *versus* the upper rotational quantum numbers and intensity ratios *versus* the CRDS
481 line positions
482 *Upper panels:* Comparison to HITRAN2016 data (mostly from [4], see Text) and Mendonca *et al.* [6].
483 Grey symbols correspond to electric quadrupolar transitions.
484 *Lower panels:* Comparison between our qSDNGP and VP line lists at 10 Torr. The deviation of the
485 positions values increasing with *J'* measures the pressure shift at 10 Torr (see Text).
486

487 The HTRAN line positions of the $^{16}O^{18}O$ isotopologue were calculated in [14] using spectroscopic
488 constants derived from a global fit of CRDS line positions measured from isotopically enriched spectra
489 and microwave [49] and Raman measurements. Again, a satisfactory agreement is achieved, maximum
490 deviations being limited to a few 10^{-4} cm^{-1} for the highest *J'* values which correspond to extremely weak
491 lines (intensity below 10^{-29} cm/molecule). The average value of the deviations is only -5.4×10^{-5} cm^{-1} (-1.6
492 MHz) while the $^{16}O^{18}O$ line intensities in natural $O_2$are less than 10^{-28} cm/molecule).

493 *4.2. Spectroscopic constantsof the $a\ ^1\Delta_g(0)$upper state*

494 The zero-pressure qSDNGP line positions were used to determine the spectroscopic constants of the
495 $a\ ^1\Delta_g(0)$ upper state of the $^{16}O_2$ and $^{16}O^{18}O$ isotopologues. The qSDNGP position values at 5 and 10 Torr
496 were used to generate a single recommended list provided as Supplementary Material. The averaged
497 position values were adopted except for the weakest lines were the 10 Torr value was preferred. The

experimental values of the upper energy level value were calculated by adding the ground state (GS) energy levels of Ref. [47] and fitted using the usual expression:

$$F(J') = E + BJ'(J'+1) - D[J'(J'+1)]^2 + H[J'(J'+1)]^3, \quad (1)$$

Where E is the energy term value, B is the rotational constant, D and H are the first- and second-order centrifugal distortion terms, respectively.

The obtained spectroscopic constants are presented in **Table 3**and the detailed lists and results of the fit are provided as a Supplementary Material. By excluding a number of less accurately determined values, a (meas.-calc.) *rms* value of 108 kHz (≈3.6×10^{-6} cm^{-1}) is achieved for $^{16}O_2$ with *J'* values between 7 and 38. As a result of larger error bars on the positions of the weak$^{16}O^{18}O$ lines, the corresponding *rms* value is about a factor of ten larger (1.23 MHz). In addition, the obtained *H* value seems to be too large compared to that of the main isotopologue and that obtained in [14] from a larger data set.

Table 3

Spectroscopic constants of the *v*=0 level of the $a^1\Delta_g$ state.

	$^{16}O_2$		**$^{16}O^{18}O$**	
	This work	Microwave. [49]	This work	Microwave [49]
E	7883.5107617(30)		7885.545863(38)	
B	1.417839009(16)	1.417839 0445(27)	1.33913386(32)	1.339135 0746(75)
D	5.102390(25)×10^{-6}	5.102338(85)×10^{-6}	4.54680(76)×10^{-6}	4.55084(22)
H	-2.297(11)×10^{-12}	-2.295(58)×10^{-12}	-4.35(50)×10^{-12}	
nb of lines	37/62	19	31/62	10
$J'_{min} - J'_{max}$	7−38	2-31	7−31	2-19
rms	3.6×10^{-6} cm^{-1} (~108 kHz)	1.03×10^{-6} cm^{-1} (31 kHz)	4.1×10^{-5} cm^{-1} (1.23 MHz)	1.40×10^{-6} cm^{-1} (42 kHz)

It is interesting to discuss the obtained parameters in relation of the results reported in [49] from microwave measurements of rotational lines in the *v*=0 level of the $a^1\Delta_g$ state for various O_2isotopologues. Drouin *et al.* [49] reported independent isotope fit parameters for six isotopologues, in particular $^{16}O_2$ and $^{16}O^{18}O$ (see **Table 3)**. Due to the higher precision of the microwave measurements, smaller standard deviations are achieved but the overall agreement is very satisfactory. These microwave data were considered in [47] to determine the energy levels of the *v*= 0 level of the $a^1\Delta_g$ state, used to compute the HITRAN line positions. Apart from the constant shift between our positions and HITRAN values (**Fig. 9**), the deviation observed for high *J* values might be related to the fact that the microwave measurements were limited to maximum *J* values of 31 while our input data set extends up to 38.

Note that the achieved *rms* of the fits is significantly smaller than the uncertainty on the GS energy levels used to compute our upper state energy levels (up to around 10^{-4} cm^{-1} for the *J*= 38 levels of $^{16}O_2$ [47]). The derived constants have then an effective character and will be possibly refined when the accuracy of the GS levels will be improved. The present measurements limited to the high energy region

of the band do not allow for a sufficient number of GS combination relations to improve the GS spectroscopic constants. Nevertheless, this goal should become achievable when the spectrum of the entire band will have been recorded.

4.3. Line intensities

The HITRAN2016 line intensities have different sources: *(i)* M1 line intensities are calculated values obtained by Orr-Ewing on the basis of FTS intensities measured in [19] completed by values obtained by Mackie using a global intensity model for the very weak lines [50], *(ii)* quadrupolar line strength were calculated in [51], *(iii)* for the minor isotopologues, calculated values from [14] and [50] are used.

The qSDNGP/HITRAN2016 intensity ratios presented in **Fig. 9**, show that HITRAN intensities of the $^{16}O_2$ M1 lines are underestimated by about 2 % for the strongest lines and up to 5% for the weakest measured lines. As concerned TS and RS quadrupole lines, a good agreement is noted for the TS lines. A systematic overestimation of the HITRAN RS line intensities by about 8 % is apparent but should be confirmed as all the considered RS line are extremely weak (intensity smaller than 5×10^{-29} cm/molecule).

Fig. 9 includes the comparison with the very recent work by Mendonca *et al.* [6] obtained by line-by-line SDVP fitting of air-broadened CRDS spectra. A multispectrum treatment was applied to spectra acquired at pressure of 495, 742.5.0 and 982.6 Torr. A very good agreement (better than 1 %) is noted between the intensity values derived by Mendonca *et al.* and our values.

4.4. Line profile parameters

As mentioned above, previous line profile studies of the $a^1\Delta_g - X^3\Sigma_g^-$ band in pure O_2 are scarce (see **Table 4**) and were performed by FTS using a Voigt profile. The value of the self-broadening parameter (Γ_0) reported in [20, 21] are overestimated. The most complete FTS study of the line-broadening was performed by Newman *et al.* [19] and includes the determination of the temperature exponent from spectra recorded at 294, 243 and 200 K for *N"* values up to 23. The empirical law estimated from their results at 294 K shows a good agreement with our results (see **Table 4**).

Table 4
Comparison to literature values of the self-broadening (Γ_0) and self-pressure shift (Δ_0) of the $a^1\Delta_g - X^3\Sigma_g^-$ O_2 band.

	Γ_0 (cm^{-1} $Torr^{-1}$)	Δ_0 (cm^{-1} $Torr^{-1}$)
Lafferty1998 [20]	$1.37(10)\times10^{-4}$	
Cheah2000 [21]	$1.03(7)\times10^{-4}$	$-4.6(2.1)\times10^{-7}$
Hill2003 [22]		$\lvert\Delta_0\rvert < 2.6\times10^{-6}$
Newman2000 [19]	7.5×10^{-5}-$1.05\times10^{-7}N"$ [a]	
This work	7.28×10^{-5}-$8.67\times10^{-7}J'$ [b]	9.93×10^{-7}-$8.44\times10^{-8}J'$ [b]

Note
[a] *Empirical expression estimated from Fig. 5 of [19].*
[b] *See Section 3.2 and Fig. 8*

Two sources are used in HITRAN2016 for the self-collisional broadening values of the the 1.27 μm band under study. Both are related to the A-band: *(i)* Brown and Plymate performed a series of FTS recordings with pure O_2 and air and determine the corresponding broadening coefficients [24], *(ii)* Washenfelder *et al.* [4], increased by 1.5% the values from Yang *et al.* [52] to better reproduce their FTS atmospheric spectra of the 1.27 μm O_2 band. While self-collisional broadening coefficients were determined in [24], atmospheric spectra provided information about air-collisional broadening coefficients and it is unclear how the air-coefficients of Ref. [4] were converted to self-collisional broadening coefficients in HITRAN2016. Nevertheless, in the case of the A-band, the differences between self- and air-broadening coefficients are small [23] and according to the FTS study of the 1.27 μm band by Newman *et al.* "The effects of pressure broadening of lines by N_2 are indistinguishable from those for pure O_2 at the same temperature and pressure" [19]. The comparison of HITRAN values to our values included in **Fig. 8** shows a very good agreement, thus indicating that the broadening coefficients in the A-band and in the 1.27 μm band are very close.

The self-pressure shift is very small in the considered band (about one order of magnitude smaller than in the A-band [23]) and thus difficult to measure: Δ_0 decreases from $+1\times10^{-6}$ to -2×10^{-6} $cm^{-1}Torr^{-1}$ when *J'* increases from 0 to 35 (see **Fig. 8**). Only an upper limit of its magnitude (2.6×10^{-6} $cm^{-1}Torr^{-1}$) could be reported from FTS recordings with O_2 pressures up to 3 atm [22]. From recordings at 1.06 bar, Cheah *et al.* retrieved a very approximate constant value ($-4.6(2.1)\times10^{-7}cm^{-1}$ $Torr^{-1}$ [21]) which is reasonable when compared to our measurements.

Self-pressure shifts are not included in the HITRAN database. We have included in **Fig. 8** the HITRAN values of the air-pressure shifts values taken from [4] and thus relative to the A-band. The magnitude of our self-pressure shifts in the 1.27 μm band is considerably smaller. The values reported by Mendonca *et al.* [6] from air-broadened CRDS spectra in the same 1.27 μm band have also a much larger amplitude. Although the values of Mendonca *et al.* were obtained from spectra recorded at much higher pressure than ours and analyzed with a different line profile (SDVP against qSPNGP), the most probable explanation of the observed differences between self- and air-shifts values in the 1.27 μm band is that the O_2-shifts have a significantly smaller amplitude than the N_2 shifts. This is indeed what was evidenced in the A-band (see Fig. 11 in [23]).

5. Concluding remarks

The first profile analysis of lines of the O_2 $a\ ^1\Delta_g - X\ ^3\Sigma_g^-(0-0)$ band in pure O_2 has been performed by CRDS coupled to a self-referenced frequency comb. The sensitivity of the recordings (α_{min}~ 10^{-12} cm^{-1}), have allowed using low pressure values and thus reducing the impact of the line profile on the determination of the zero-pressure line center and of the line intensities. In particular line mixing effects are negligible at the pressure of the recordings.Important deviations from the standard Voigt profile are

evidenced even for pressure values limited to a few Torr. The quadratic Speed-Dependent Nelkin-Ghatak profile was found to allow a satisfactory reproduction of the observed profiles. Overall, about 167 lines including electric quadrupole transitions with intensity as 10^{-30} cm/molecule were measured in the high energy part of the band accessible with the ECDL at disposal (7920-8085 cm^{-1} interval). A conservative 500 kHz accuracy is estimated for the zero-pressure line positions of isolated lines with intensity larger than 10^{-28} cm/molecule. The small self-pressure shifts of the line centers are reported for the first time. The spectroscopic constants of the $a\ ^1\Delta_g(0)$ upper state of the $^{16}O_2$ and $^{16}O^{18}O$ isotopologues were determined from a fit of the zero-pressure qSDNGP line positions. A standard deviation of 108 kHz (3.6×10^{-6} cm^{-1}) was achieved by using 37 line centers of $^{16}O_2$ corresponding to *J* values between 7 and 38. Taking into account that the values of the ground state energy levels are not known with such accuracy [47], the full spectral coverage of the considered O_2band with similar accuracy will probably allow improving not only the $a\ ^1\Delta_g(0)$ upper state constants but also the $X\ ^3\Sigma_g^-(0)$ GS constants.

Most of the measured line positions show deviations exceeding the 10^{-4} cm^{-1} error bar attached to HITRAN positions. As concerned line intensities, HITRAN values are found to be underestimated by 2-4 % compared to our values.

The next step of our CRDS study of this band will be to extend the study to the low energy region using a different CRDS spectrometer. The use of two different CRDS setups will allow checking the consistency of the claimed accuracy of the line position (estimated to be 500 kHz in the present work).A global intensity modeling including the different branches of magnetic dipole and electric quadrupole transitions will be then undertaken. Additional laboratory work is still required to fulfill the needs for remote sensing applications. It concerns in particular the air-broadened profiles, the temperature dependence of the line profile parameters (and of the CIA) and line mixing effects which have an important impact at atmospheric pressures remain to be characterized in particular in the region of the *Q* branch.

Acknowledgements

M. K acknowledges financial support from the French Embassy in Poland. This work was performed in the frame of the LabexOSUG@2020 (ANR10 LABX56). A partial support from CNES is acknowledged. We are grateful to the reviewers for their useful and constructive suggestions.

References

[1] D. A. Long, D. K. Havey, M. Okumura, C. E. Miller and J. T. Hodges,J. Quant. Spectrosc. Radiat. Transfer **111**, 2021-36 (2010).
O_2 A-band line parameters to support atmospheric remote sensing.
doi.org/10.1016/j.jqsrt.2010.05.011

[2] J.-L. Bertaux, A. Hauchecorne, F. Lefèvre, D. Jouglet, L. Blanot, F.-M. Bréon, P. Akaev, and P. Lafrique, Geophys. Res. Abstracts **20**, EGU2018-14935, EGU General Assembly (2018).
Use of the 1.27 μm O_2 absorption band for CO_2 and methane estimates in nadir viewing from space: Potential and application to Microcarb.

[3] K. Sun, I. E. Gordon, C. E. Sioris, X. Liu, K. Chance and S. C. Wofsy, The combined 15th HITRAN and 14th ASA conference (Cambridge, MA) (2018).
Re-evaluating the use of O_2 $a^1\Delta_g$ band in the spaceborne remote sensing of greenhouse gases

[4] R. A. Washenfelder, G. C. Toon, J.-F. Blavier, Z. Yang, N. T. Allen, P. O. Wennberg, S. A. Vay, D. M. Matross and B. C. Daube, J. Geophys. Res. **111**, D22305 (2006).
Carbon dioxide column abundances at the Wisconsin Tall Tower site

[5] D. Wunch, G. C. Toon, J.-F. L. Blavier, R. A. Washenfelder, J. Notholt, B. J. Connor, D. W. T. Griffith, V. Sherlock and P. O. Wennberg, Philosoph. Trans. Royal Soc. A **369**, 2087–2112 (2011).
The Total Carbon Column Observing Network.
doi.org/10.1098/rsta.2010.0240

[6] J. Mendonca, K. Strong, D. Wunch, G. C. Toon, D. A. Long, J. T. Hodges, V. T. Sironneau and J. E. Franklin, Atmos. Meas. Tech. Discuss. **12**, 35-50 (2019).
Improving the Retrieval of XCO_2 from Total Carbon Column Network Solar Spectra
doi.org/10.5194/amt-2018-62

[7] microcarb.cnes.fr/en

[8] R. M. Goody and Y. L. Yung, Second edition. Oxford University Press, New York, **xvi, 519** (1989) Science **247**, 4941, 476-476 (1990).
Atmospheric Radiation. Theoretical Basis
doi.org/10.1126/science.247.4941.476

[9] I.E. Gordon, L. S. Rothman, C. Hill, R. V. Kochanov, Y. Tan, P. F. Bernath, M. Birk, V. Boudon, A.Campargue, K. V. Chance, B. J. Drouin, J.-M. Flaud, R. R. Gamache, J. T. Hodges, D. Jacquemart, V. I. Perevalov, A. Perrin, K. P. Shine, M.-A. H. Smith, J. Tennyson, G. C. Toon, H. Tran, V. G. Tyuterev, A. Barbe, A. G. Császár, V. M. Devis, T. Furtenbacher, J. J. Harrison, J.-M. Hartmann, A. Jolly, T. J. Johnson, T. Karman, I. Kleiner, A. A. Kyuberis, J. Loos, O. M. Lyulin, S. T. Massie, S. N. Mikhailenko, N. Moazzen-Ahmadi, H. S. P. Müller, O. V. Naumenko, A.V. Nikitin, O. L. Polyansky, M. Rey, M. Rotger, S. W. Sharpe, K.Sung, E. Starikova, S.A.Tashkun, J. Vander Auwera, G. Wagner, J. Wilzewski, P.Wcisło, S. Yu and E.J. Zak, J. Quant. Spectrosc. Radiat. Transfer**203**, 3-69 (2017).
The HITRAN2016 Molecular Spectroscopic Database.
doi.org/10.1016/j.jqsrt.2017.06.038

[10] E. J. Mlawer, S. A. Clough, P. D. Brown, T. M. Stephen, J. C. Landry, A. Goldman, F. J. Murcray, J. Geophys. Res.: Atmos. **103**, 3859-63 (1998).
Observed atmospheric collision-induced absorption in near-infrared oxygen bands
doi.org/10.1029/97JD03141

[11]S. Solomon, R. W. Portmann, R. W. Sanders, J. S. Daniel, J. Geophys. Res.: Atmos. **103**, 3847-58 (1998).
Absorption of solar radiation by water vapor, oxygen, and related collision pairs in the Earth's atmosphere
doi.org/10.1029/97JD03285

[12] A. Misra, V. Meadows, M. Claire, et al. Astrobiology **14**,67–86 (2014).
Using dimers to measure biosignatures and atmospheric pressure for terrestrial exoplanets.

[13] O. Leshchishina, S. Kassi, I. E. Gordon, L. S. Rothman, L. Wang and A. Campargue, J. Quant. Spectrosc. Radiat. Transfer **111**, 2236-45 (2010).
High sensitivity CRDS of the $a^1\Delta_g$ - $X^3\Sigma_g^-$ band of oxygen near 1.27 μm: extended observations, quadrupole transitions, hot bands and minor isotopologues

[14] O. Leshchishina, S. Kassi, I. E. Gordon, S. Yu and A. Campargue, J. Quant. Spectrosc. Radiat. Transfer **112**, 1257-65 (2011).
The $a^1\Delta g - X^3\Sigma$-g band of $^{16}O^{17}O$, $^{17}O^{18}O$ and $^{17}O_2$ by high sensitivity CRDS near 1.27 μm
doi.org/10.1016/j.jqsrt.2010.05.014

[15] D. Mondelain, S. Kassi and A. Campargue, J. Geophys. Res.: Atmos. **124**, 1, 414-423 (2019).
Accurate laboratory measurement of the O_2 collision-induced absorption band near 1.27 μm
doi.org/10.1029/2018JD029317

[16] B. Maté, C. Lugez, G. T. Fraser and W. J. Lafferty, J. Geophys. Res.: Atmos. **104**, D30585(1999).
Absolute intensities for the O_2 1.27 μm continuum absorption.
https://doi.org/10.1029/1999JD900824

[17] I.E. Gordon, S. Kassi, A. Campargue and G. C. Toon, J. Quant. Spectrosc. Radiat. Transfer**111**, 1174-83 (2010).
First identification of the $a^1\Delta_g$ - $X\ ^3\Sigma_g^-$ electric quadrupole transitions of oxygen in the solar and laboratory spectra

[18] S. Kassi,O. Leshchishina, I. E. Gordon, S. Yu and A. Campargue, Chem. Phys. Lett. **502** 37-41 (2011).
Hyperfine structure of the $a^1\Delta_g$ - $X\ ^3\Sigma_g^-$ transitions of $^{16}O^{17}O$, $^{17}O^{18}O$ and $^{17}O_2$ by CRDS at 80 K.

[19] S. M. Newman, A. J. Orr-Ewing, D. A. Newnham and J. Ballard, J. Physic. Chem. A1049467 (2000).
Temperature and pressure dependence of line widths and integrated absorption intensities for the O_2 $a^1\Delta_g$ - $X^3\Sigma_g$ - (0,0) transition

[20] W. J. Lafferty, A. M. Solodov, C. L. Lugez and G. T. Fraser, Appl. Opt. **37**, 2264-70 (1998).
Rotational Line Strengths and Self-Pressure-Broadening Coefficients for the 1.27 μm, $a^1\Delta_g$ - $X\ ^3\Sigma_g^-$ (0,0) Band of O_2.

[21] S.-L. Cheah, Y.-P. Lee and J. F. Ogilvie, J. Quant. Spectrosc. Radiat. Transfer**64**, 467 (2000).
Wavenumbers, strengths, widths and shifts with pressure of lines in four bands of gaseous $^{16}O_2$ in the systems $a^1\Delta_g$ - $X\,^3\Sigma_g^-$'and $b\,^1\Sigma_g^+$ - $X\,^3\Sigma_g^-$

[22] C. Hill, J. M. Brown and D. A. Newnham, J. Molec. Spectrosc. **221**, 286-287 (2003).
An upper limit for the magnitude of pressure shifts in the O_2 $a^1\Delta_g$ - $X^3\Sigma_g$ - (0,0) band
https://doi.org/10.1016/S0022-2852(03)00227-3

[23] B. J. Drouin, D. Ch. Benner, L. R. Brown, M. J. Cich, T. J. Crawford, V. Malathy Devi, A. Guillaume, J. T. Hodges, E. J. Mlawer, D. J. Robichaud, F. Oyafuso, V. H. Payne, K. Sung, E. H. Wishnow and S. Yu, J. Quant. Spectrosc. Radiat. Transfer **186**, 118-138 (2017).
Multispectrum analysis of the oxygen A-band,
https://doi.org/10.1016/j.jqsrt.2016.03.037

[24] L.R. Brown and C. Plymate, J. Molec. Spectrosc. **199**, 166-179 (2000).
Experimental line parameters of the oxygenA-band at 760 nm

[25] P. Maddaloni, P. Malara, E. De Tommasi, M. De Rosa, I. Ricciardi, G. Gagliardi, F. Tamassia, G. Di Lonardo, and P. De Natale, J. Chem. Phys. **133**, 154317 (2010)
Absolute measurement of the S(0) and S(1) lines in the electric quadrupole fundamental band of D_2 around 3 μm
doi.org/10.1063/1.3493393

[26] J. Domysławska, S. Wójtewicz, D. Lisak, A. Cygan, F. Ozimek, K. Stec, Cz. Radzewicz, R. S. Trawiński and R. Ciuryło, J. Chem. Phys. **136**, 024201 (2012).
Cavity ring-down spectroscopy of the oxygen B-band with absolute frequency reference to the optical frequency comb
doi.org/10.1063/1.3675903

[27] D. C. Benner, C. P. Rinsland, V. M. Devi, M. A. H. Smith and D. Atkins, J. Quant. Spectrosc. Radiat. Transfer**53**, 705 (1995)
A multispectrum nonlinear least squares fitting technique
doi.org/10.1016/0022-4073(95)00015-D

[28] A. S. Pine and R. Ciuryło, J. Mol. Spectrosc. **208**, 180 (2001)
Multispectrum Fits of Ar-Broadened HF with a Generalized Asymmetric Lineshape: Effects of Correlation, Hardness, Speed Dependence, and Collision Duration
doi.org/10.1006/jmsp.2001.8375

[29] D. Romanini, A. A. Kachanov, N. Sadeghi and F. Stoeckel, Chem. Phys. Lett. **264**, 316-322 (1997).
CW cavity ring down spectroscopy
10.1016/S0009-2614(96)01351-6

[30] P. Macko, D. Romanini, S. N. Mikhailenko, O. V. Naumenko, S. Kassi, A. Jenouvrier, V. G. Tyuterev and A. Campargue, J. Mol. Spectrosc.**227**, 90-108 (2004).
High sensitivity CW-cavity ring down spectroscopy of water in the region of the 1.5 μm atmospheric window
10.1016/j.jms.2004.05.020

[31] S. Kassi and A. Campargue, J. Chem. Phys. **137**, 234201 (2012).
Cavity Ring Down Spectroscopy with 5×10^{-13} cm^{-1} sensitivity

doi.org/10.1063/1.4769974

[32] A. Campargue, S. Kassi, K. Pachucki and J. Komasa, Phys. Chem. Chem. Phys. **14**(2), 802–815 (2012).
The absorption spectrum of H_2: CRDS measurements of the (2-0) band, review of the literature data and accurate ab initio line list up to 35000 cm^{-1}
10.1039/C1CP22912E

[33] D. Mondelain, S. Kassi, T. Sala, D. Romanini, M. Marangoni and A. Campargue,J. Mol. Spectrosc. **326**, 5–8 (2016).
Sub-MHz accuracy measurement of the S(2) 2–0 transition frequency of D_2 by comb-assisted cavity ring down spectroscopy
doi:10.1016/j.jms.2016.02.008

[34] D. Mondelain, S. N. Mikhailenko, E. V. Karlovets, S. Béguier, S. Kassiand A. Campargue, J. Quant. Spectrosc. Radiat. Transfer **203**, 206–212 (2017).
Comb-Assisted Cavity Ring Down Spectroscopy of ^{17}O enriched waterbetween 7443 and 7921 cm^{-1}
10.1016/j.jqsrt.2017.03.029

[35] S. N. Mikhailenko, D. Mondelain, E. V. Karlovets, S. Kassiand A. Campargue,J. Quant. Spectrosc. Radiat. Transfer **206**, 163-171 (2018).
Comb-Assisted Cavity Ring Down Spectroscopy of ^{17}O enriched waterbetween 6667 and 7443 cm^{-1}
doi.org/10.1016/j.jqsrt.2017.10.023

[36] T. Stoltmann, M. Casado, M. Daëron, A. Landais and S. Kassi, Analyt. Chem.**89**(19), 10129-32 (2017).
Direct, Precise Measurements of Isotopologue Abundance Ratios in CO2 Using Molecular Absorption Spectroscopy: Application to $\Delta^{17}O$
10.1021/acs.analchem.7b02853

[37] L. Galatry, Phys. Rev. **122**, 1218–23 (1961).
Simultaneous effect of Doppler and foreign gas broadening on spectral lines.
doi.org/10.1103/PhysRev.122.1218

[38] M. Nelkin and A. Ghatak, Phys. Rev. **135**, A4–9 (1964).
Simple binary collision model for Van Hove's $G_s(r,t)$
doi.org/10.1103/PhysRev.135.A

[39] S. G. Rautian and I. I. Sobel'man,Sov. Phys. Usp. **9**, 701–16 (1967).
The effect of collisions on the Doppler broadening of spectral lines
doi.org/10.1070/PU1967v009n05ABEH003212

[40] P. R. Berman, J. Quant. Spectrosc. Radiat. Transfer **12**,1331–42 (1972).
Speed-dependent collisional width and shift parameters in spectral profiles.

[41] B. Lance, G. Blanquet, J. Walrand and J-P. Bouanich, J. Mol. Spectrosc. **185**, 262–71 (1997).
On the speed-dependent hard collision line shape models: application to C_2H_2 perturbed by Xe.
doi.org/10.1006/jmsp.1997.7385

[42] A. S. Pine, J. Quant. Spectrosc. Radiat. Transfer **62**, 397–423 (1999).
Asymmetries and correlations in speed-dependent Dicke-narrowed line shapes of argon-broadened HF.

821 doi.org/10.1016/S0022-4073(98)00112-5
822 [43] J. Tennyson, P. F. Bernath, A. Campargue, A. G. Császár, L. Daumont, R. R. Gamache, J.T. Hodges,
823 D. Lisak, O. V.Naumenko, L. S. Rothman, H. Tran, N. F. Zobov, J. Buldyreva, C. D. Boone,
824 M. D. De Vizia, L. Gianfrani, J.-M. Hartmann,R. McPheat, D. Weidmann, J. Murray, N. Hoa Ngo and
825 O. L. Polyansky, Pure Appl. Chem. **86**(12): 1931–43IUPAC Technical Report (2014)
826 *Recommended isolated-line profile for representing high-resolution spectroscopic transitions (IUPAC*
827 *Technical Report)*
828
829 [44] R.H. Dicke, Phys. Rev. **89**, 472–3 (1953).
830 *The effect of collisions upon the Doppler width of spectral lines.*
831 doi.org/10.1103/PhysRev.89.472
832

833 [45] Priem D, Rohart F, Colmont J-M, Wlodarczak G, Bouanich J-P. J Mol Struct. **517**, 435–54
834 (2000)*Lineshape study of the J ¼ 3'2 rotational transition of CO perturbed by N_2 and O_2.*
835 http://dx.doi.org/10.1016/S0022-2860(99)00268-9.
836
837 [46] Wójtewicz S, Cygan A, Masłowski P, Domysławska J, Lisak D, Trawinski RS,et al. J Quant
838 Spectrosc Radiat Transf. **144**, 36–48 (2014).
839 *Spectral line shapes of self-broadened P-branch transitions of oxygen B band.*
840 http://dx.doi.org/10.1016/j.jqsrt.2014.03.029.
841
842 [47] S. Yu, B. J. Drouin and C. E. Miller, J. Chem. Phys. **141**,174302 (2014).
843 *High resolution spectral analysis of oxygen. IV. Energy levels, partition sums, band constants, RKR*
844 *potentials, Franck-Condon factors involving the $X^3\Sigma^-_g$, $a^1\Delta_g$ and $b^1\Sigma^+_g$ states*
845 doi.org/10.1063/1.4900510.
846
847 [48] C. Amiot and J. Verges, Can. J. Phys. **59(10)**, 1391-8 (1981).
848 *The magnetic dipole $a^1\Delta_g \rightarrow X^3\Sigma_g^-$ transition in the oxygen afterglow*
849 doi.org/10.1139/p81-183
850
851 [49] B. J. Drouin, H. Gupta, S. Yu, C. Miller, and H.S.P. Müller, J. Chem. Phys. **137**,024305 (2012).
852 *High resolution spectral analysis of oxygen. II. Rotational spectra of $a^1\Delta_g$O2 isotopologues*
853 doi.org/10.1063/1.4719169]
854
855 [50] C. Mackie, Global intensity model, private communication (2011).
856
857 [51] A. P. Mishra, T. K. Balasubramanian and B. J. Shetty, J. Quant. Spectrosc. Radiat. Transfer **112**,
858 2303-9 (2011).
859 *Generalized electric quadrupole branch line strengths for the infrared atmospheric oxygen bands*
860
861 [52] Z. Yang, P.O. Wennberg, R.P. Cageao, T.J. Pongetti, G.C. Toon, and S.P. Sander,
862 J. Quant. Spectrosc. Radiat. Transfer **90**, 309–21 (2005).
863 *Ground-based photon path measurements from solar absorption spectra of the O_2 A-band,*
864 doi.org/10.1016/j.jqsrt.2004.03.020.

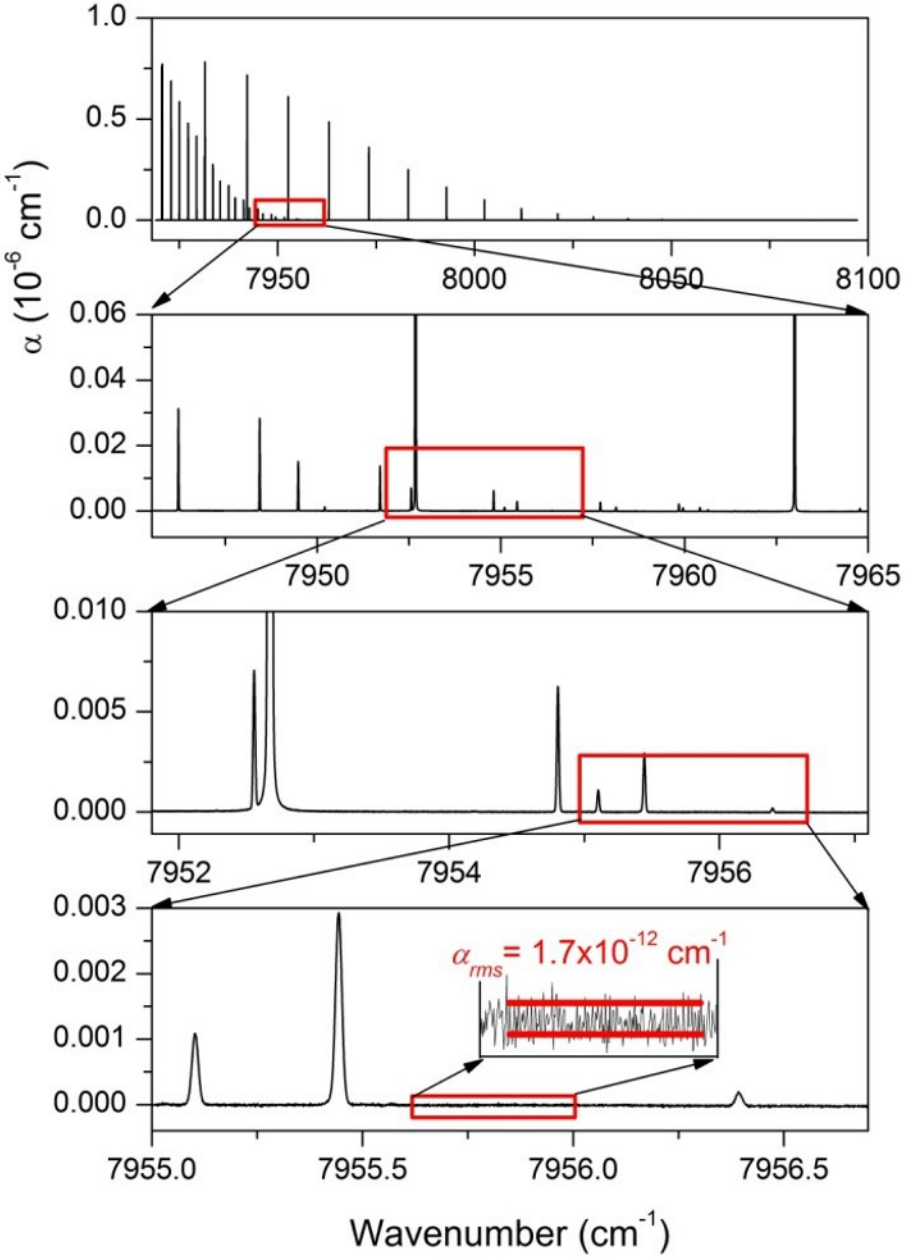
α (10^-6 cm^-1)
1.0
0.5
0.0
7950
8000
8050
8100
0.06
0.04
0.02
0.00
7950
7955
7960
7965
0.010
0.005
0.000
7952
7954
7956
0.003
0.002
0.001
0.000
α_rms = 1.7x10^-12 cm^-1
7955.0
7955.5
7956.0
7956.5
Wavenumber (cm^-1)

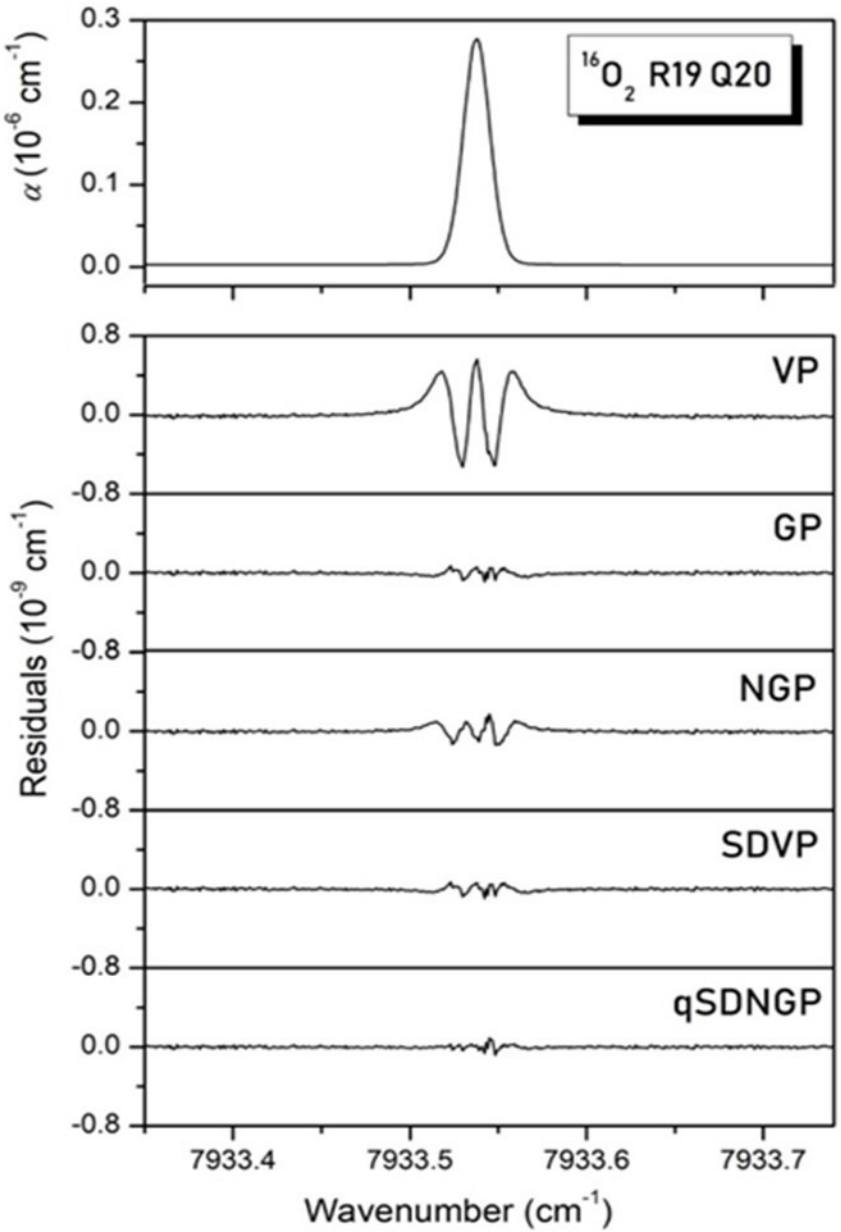
α (10^-6 cm^-1)
0.3
0.2
0.1
0.0
16O2 R19 Q20
Residuals (10^-9 cm^-1)
0.8
0.0
-0.8
VP
GP
NGP
SDVP
qSDNGP
7933.4
7933.5
7933.6
7933.7
Wavenumber (cm^-1)